nature geoscience

Article

https://doi.org/10.1038/s41561-025-01697-1

Increased plant productivity exacerbates subsoil carbon losses under warming via nitrogen mining

Received: 8 August 2024

Accepted: 7 April 2025

Published online: 7 May 2025

Check for updates

Mingming Wang[1,2], Shuai Zhang[1,2], Guocheng Wang[3], Liujun Xiao[4], Baojing Gu[1,2], Mianhai Zheng[5], Shuli Niu[6], Yuanhe Yang[7], Yiqi Luo[8], Ganlin Zhang[9], Zhou Shi[1,2] & Zhongkui Luo[1,2]

Soils can be either a source or sink of atmospheric CO_2 depending on how soil organic carbon (SOC) responds to climate warming and changes in plant productivity. Whereas warming typically accelerates SOC decomposition, the effect of plant productivity changes remains unclear. Here we use a space-for-change substitution approach to analyse a global dataset of SOC measurements down to 1 metre. We find that warming-induced SOC reduction in the 0–0.3-m topsoil is gradually offset by increasing plant productivity but exacerbated in the 0.3–1-m subsoil until plant productivity increase crosses a threshold of 30%. Consequently, entirely offsetting warming-induced SOC reduction in the top metre of soil requires an unrealistically high increase in plant productivity, albeit with substantial variance across ecosystems. Soil carbon-to-nitrogen ratio is the dominant predictor of the variance in SOC response, as this ratio determines whether nitrogen released during carbon loss meets the requirement for additional plant growth or whether additional nitrogen must be mined from soil organic matter. Such mining accelerates SOC losses, particularly in the subsoil, where the soil carbon-to-nitrogen ratio is lower than in topsoils. We conclude that globally, increased plant productivity may exacerbate SOC losses under climate warming, particularly in the subsoil.

Soil organic carbon (SOC) stores twice as much carbon as the atmosphere and upland vegetation combined, making it the largest terrestrial organic carbon pool[1]. Under global change, SOC can be either a sink or source, depending on the balance between carbon inputs (primarily from plant productivity) and outputs (via microbial decomposition). Climate warming is anticipated to stimulate microbial decomposition, increasing SOC losses[2–4]. Conversely, plant productivity, the primary source of SOC inputs, responds dynamically to warming and other global changes such as elevated atmospheric CO_2 concentration (eCO_2), nitrogen deposition, shifting fire regimes and lengthening growing seasons[5–7]. However, the joint effects of warming and plant productivity changes on whole-profile SOC balance remain poorly understood, particularly across large spatial extents and long timescales[8].

Plant productivity can be enhanced by global change such as the CO_2 fertilization effect and increased nitrogen availability[9–11]. This leads to increased carbon inputs into the soil, counteracting warming-induced SOC losses. Nevertheless, empirical evidence supporting this counteraction effect is limited, and decreased SOC storage under increased plant growth has even been found[12]. One proposed reason for this phenomenon is soil nutrient mining triggered by enhanced plant growth, particularly in nitrogen-limited systems[13]. That is, plant growth enhancement extracts nutrients (primarily nitrogen) from soil organic matter by stimulating its decomposition to support additional

A full list of affiliations appears at the end of the paper. e-mail: luozk@zju.edu.cn

https://doi.org/10.1038/s41561-025-01697-1

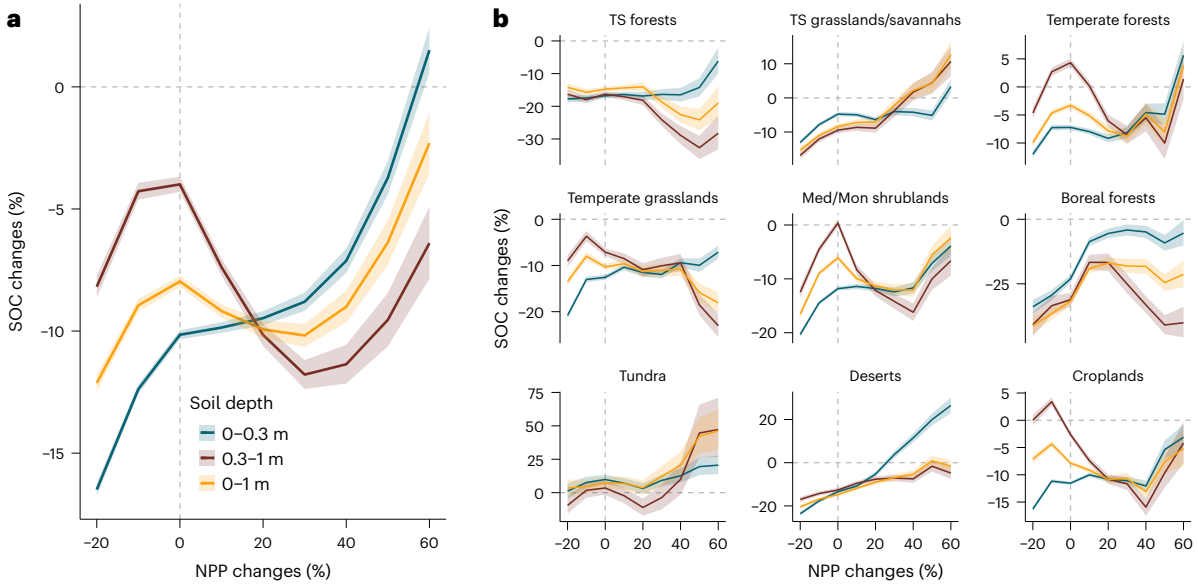

Fig. 1 | The responses of SOC to changes in NPP under 1.5 °C warming. a, Global average responses in different soil depth layers. **b**, Ecosystem-specific responses. The coloured lines show the mean response. The shading envelope represents the 95% confidence interval. TS forests, tropical/subtropical forests; Med/Mon shrublands, Mediterranean/montane shrublands; TS grasslands/savannahs, tropical/subtropical grasslands/savannahs.

growth[12]. This alters soil carbon–nitrogen coupling and nutrient cycling processes[5,14,15]. However, soil nutrient conditions vary substantially over space, both horizontally across the globe and vertically along the soil profile[16]. Soils with low carbon-to-nitrogen ratio (CNR), indicating more nutrient per unit carbon, may release more nutrients per unit decomposition of soil organic matter, thereby supporting greater additional plant growth compared to high CNR soils. Given the close association of the decomposition of soil organic matter with temperature, simultaneous plant productivity changes and warming may have unforeseen consequences on SOC dynamics, which cannot be predicted by their individual effects alone[17,18].

Furthermore, warming may result in deeper rooting depths of plants, allowing them to access subsoil water and nutrient resources[19,20]. This increase in subsoil root biomass can destabilize SOC through processes such as aggregate destruction or organic acid exudation, reducing the physical separation between microbes and SOC, destabilizing protected carbon and alleviating microbial energy limitation at depth, all of which can promote deep SOC decomposition[21]. In particular, under the continuous variation of nutrient and hydrothermal conditions brought about by global change, plant community composition may shift. This shift can lead to changes in the stoichiometry (for example, carbon-to-nutrient ratio) of live biomass and plant detritus and in root distribution along the soil profile. These changes may result in nonlinear SOC responses to global change factors, depending on the changes in the magnitude of stoichiometry and root systems of the plant community. The consequences of these below-ground, nonlinear and interactive effects on SOC dynamics may only become apparent on long timescales and can vary widely across space, especially considering that the timescale of SOC turnover often spans decades or even millennia[22,23]. Novel approaches are needed to address the combined effects of alterations in plant growth, potential community shifts, plant nutrient acquisition and SOC decomposition on long-term, large-scale, whole-profile SOC storage.

Here we analysed a global dataset of SOC stocks down to 1 m at 124,123 sites[24] (Extended Data Fig. 1) and utilized satellite-[25] and field-survey-derived estimates of vegetation net primary productivity (NPP)[26]. Our goal was to quantify the response of whole-profile SOC to simultaneous warming and plant productivity changes on a global scale, while also exploring the underlying mechanisms. To achieve this, we employed a hybrid approach combining space-for-change substitution with meta-analysis techniques[4]. Briefly, SOC values at sites with the same mean annual temperature (MAT) and NPP (that is, the ambient group) was compared with SOC values at sites (that is, the changing group) with specific changes in MAT (1.5 °C increase in this study) and NPP (ranging from −20% to +60% in 10% increments, reflecting empirical observations and projections of Earth system models and acknowledging potential uncertainties in NPP changes under climate change[27–29]). At the same time, confounding factors such as precipitation, precipitation seasonality, soil type and landform were controlled, ensuring that they were the same between the two groups (Extended Data Fig. 2). Consequently, the primary difference between the two groups of soil sites was in MAT and NPP, and the difference of SOC stocks between the two groups (ΔSOC) can be attributed to these two factors (Methods). This comparison assumes that SOC in the same ambient group will eventually reach a state comparable to that of the changing group. As the dataset covers diverse climate, soil and vegetation conditions globally (Extended Data Fig. 1), combined with meta-analysis techniques, the approach enables a comprehensive evaluation of ΔSOC across different soil depth layers (0–0.3, 0.3–1 and 0–1 m in this study) as impacted by warming and NPP changes, in relation to other environmental conditions (Methods).

Global and ecosystem responses of SOC

Averaged across the globe, the percentage change in SOC stock (ΔSOC) under 1.5 °C air warming without productivity changes is −10.2% (−10.3%, −9.9%) (mean with 95% confidence interval) in the 0–0.3, −4.0% (−4.3, −3.7%) in 0.3–1 m and −8.0% (−8.2, −7.7%) in 0–1 m depth (Fig. 1a). These different percentage changes support depth-dependent temperature sensitivity of SOC decomposition, which may result from the vertical gradients of soil physico-chemical properties and carbon quality and availability[2,21]. However, we should note that air warming is not equal to soil warming. If soil temperature does not change synchronically with air warming (albeit this would rarely occur over climatic timescales[30]), we should use caution using these different percentage changes induced by air warming to infer the temperature sensitivity of SOC in different soil depth layers.

In the top 0–0.3 m of soil, SOC changes are positively and linearly correlated with increasing NPP (Fig. 1a), leading to a gradual

https://doi.org/10.1038/s41561-025-01697-1

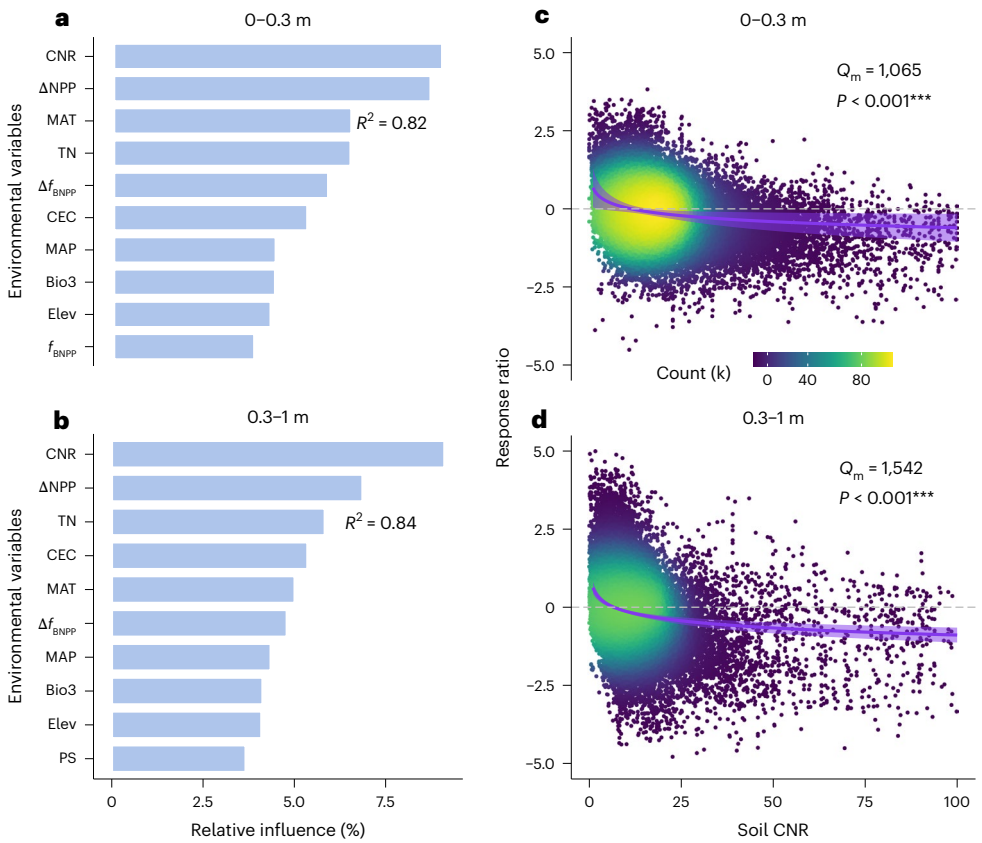

Fig. 2 | Drivers of the responses of SOC to plant productivity changes and warming. a,**b**, The most important ten environmental factors and their relative influence on the response ratio of topsoil (**a**) and subsoil (**b**) SOC to plant productivity changes and warming. A detailed description of the environmental factors is shown in Supplementary Table 1. **c**,**d**, The relationship between the response ratio and soil CNR in the topsoil (**c**) and subsoil (**d**). The purple line is the fitted meta-regression line with the shading envelope showing the 95% confidence interval. Q_m, Q value of the importance of CNR from the meta-regression. The grey dashed horizontal line represents no changes in SOC (that is, the response ratio = 0). Count represents the data density. TN, total soil nitrogen content; CEC, cation exchange capacity; Bio3, isothermality; Elev, elevation; f_{BNPP}, the fraction of below-ground NPP.

counteraction of warming-induced SOC reduction. Subsoil (0.3–1 m) SOC, on the other hand, exhibits a nonlinear relationship with NPP changes, characterized by a multi-phase response (Fig. 1a). Warming-induced SOC reduction intensifies with increasing NPP until the NPP increase crosses a tipping point of 30%. Beyond this point, further SOC reduction halts, and SOC changes exhibit a positive association with increasing NPP. However, warming-induced subsoil SOC losses cannot be entirely offset even with a 60% (which is the highest NPP increase scenario in our assessment) NPP increase (Fig. 1a).

In the whole 1-m soil depth, due to the distinct responses of topsoil and subsoil SOC to NPP changes, especially the opposing responses under relatively low NPP changes, SOC loss is exacerbated by NPP increases under warming under low NPP changes (< 30%; Fig. 1a). Averaging globally, similarly to the subsoil, a 60% increase in NPP also cannot entirely offset 1.5 °C warming-induced SOC loss in the whole 1-m soil (Fig. 1a), suggesting that additional NPP required to entirely offset warming-induced SOC losses would be unrealistically high. Indeed, much lower NPP changes have been observed in most Free-Air CO_2 experiments (FACE)[31,32] or predicted by Earth system models under future climate change scenarios[27,28].

Among ecosystems, similar contrasting responses of topsoil and subsoil SOC to NPP changes persist in terms of both magnitude and direction in most ecosystems (Fig. 1b). In the topsoil, specifically, a 27% increase in NPP in deserts, 54% in tropical/subtropical grasslands/savannahs and 57% in temperate forests completely offset the respective SOC reduction in topsoil. Especially, warming indeed induces SOC gains in tundra systems, and this carbon sink is further enhanced by increasing NPP (Fig. 1b). In all other ecosystems, however, a 60% increase in NPP cannot entirely offset warming-induced SOC losses (Fig. 1b).

Looking into the individual relationships between NPP and SOC changes for each ecosystem in the subsoil (Fig. 1b), it appears that global-level nonlinearity of the relationship is an aggregation of distinct relationships at the ecosystem level. In five out of the nine ecosystems (tropical/subtropical forests, temperate forests, Mediterranean/montane shrublands, tundra and croplands), NPP increase exacerbates subsoil SOC reduction until crossing a tipping point, but the tipping point value varies among the five ecosystems ranging from 20% to 50%. In boreal forests, SOC reduction is first offset but then exacerbated with increasing NPP. In tropical/subtropical grasslands/savannahs and deserts, on the contrary, SOC reduction is almost linearly counteracted by increasing NPP, albeit at distinct counteracting rates. In these arid and semi-arid ecosystems, plants may allocate more NPP to the subsoil to acquire moisture as NPP increases under warming (Extended Data Fig. 3b). This moisture acquisition, in turn, could reduce soil moisture available for microbial decomposition, thereby promoting subsoil SOC accumulation. In temperate grasslands, NPP increase continuously exacerbates SOC reduction, with a much higher exacerbating rate when NPP increase exceeds 40% (Fig. 1b). Overall, these results demonstrate distinct responses of subsoil SOC to NPP shifts among ecosystems.

Drivers of SOC responses

The differential responses of SOC across soil depths and among ecosystems may be attributed to potential changes in the vertical

https://doi.org/10.1038/s41561-025-01697-1

allocation of below-ground productivity. If plants allocate less carbon to the subsoil while allocating more to the topsoil, this could lead to much higher carbon inputs to the topsoil, thereby promoting SOC storage therein. However, we do not find a significant increase in the below-ground allocation of NPP (BNPP) to the topsoil either on the global scale (Extended Data Fig. 4a) or at the ecosystem level under the warming and NPP change scenarios (Extended Data Fig. 4b). On the contrary, globally, the proportional allocation of BNPP to the subsoil layer has increased although this increase declines with increasing NPP (Extended Data Fig. 3a), in line with observations from field warming and FACE experiments[19,20]. Among ecosystems, however, the depth allocations of BNPP show contrasting responses to NPP changes (Fig. 4b), but do not show apparent alignment with the responses of both topsoil and subsoil SOC (Fig. 1b).

To delve into the controls of ΔSOC, we fitted a machine-learning-based statistic model (random forest) driven by NPP changes (ΔNPP) and a suite of other environmental factors (Methods). The model explains >82% ($R^2 > 0.82$) of the global variance of ΔSOC both in the topsoil and subsoil (Fig. 2a,b). Soil CNR emerges as the most influential predictor, followed by ΔNPP (Fig. 2a,b). Once again, the allocation change of BNPP (Δf_{BNPP}) is relatively marginal compared to the importance of CNR (Fig. 2a,b). Additionally, total soil nitrogen content is a more important predictor than Δf_{BNPP} in the two depths. Other environmental factors (for example, baseline MAT and mean annual precipitation (MAP)) also regulate ΔSOC but are less important. This order of predictor importance suggests that soil nitrogen status plays a key role in regulating the response of SOC to NPP changes under warming and plant productivity changes.

Pooling together all ΔSOC estimates under warming and different NPP change scenarios, a linear meta-regression of ΔSOC against CNR indicates that ΔSOC is significantly negatively related to CNR in both soil layers (Fig. 2c,d). Specifically, SOC gradually shifts from accumulation to reduction with increasing CNR. Additionally, we fitted a mixed-effects meta-regression to explore the effects of CNR, ΔNPP and their interactions on ΔSOC and tested whether and how their effects vary among soil depths (Methods). Among the two soil depths, the slope of the relationship between ΔSOC and CNR is significantly steeper in the subsoil than in the topsoil (Fig. 3a), demonstrating that SOC response shows stronger association with CNR in the subsoil than in the topsoil. In line with the general pattern of ΔSOC in response to ΔNPP (Fig. 1a), ΔSOC is positively related to ΔNPP, but the slope for the topsoil is significantly steeper than that for the subsoil (Fig. 3a), suggesting that plant productivity increases provide more benefits for topsoil SOC accumulation compared to subsoil. Thus, we would like to highlight that the same amount of NPP changes may have different implications for SOC in the subsoil and topsoil. This is because the above-ground fraction of NPP (for example, litterfall) can directly contribute to topsoil SOC storage, whereas carbon inputs to the subsoil primarily come from below-ground root exudates and detritus.

It is important to note that the effect of the interaction between CNR and ΔNPP on ΔSOC is significant for both layers but opposite in terms of direction between the two depth layers (Fig. 3a). In the subsoil, the effect of the interaction is positive. That is, with increasing NPP, the negative effect of CNR weakens, and thus the positive effect of NPP gradually becomes dominant. This result well explains the multi-phase nonlinear responses of SOC to ΔNPP in the subsoil showed in Fig. 1. In the topsoil, however, the positive effect of NPP is stronger (Fig. 3a); it may always outweigh the negative effect of CNR, leading to the monotonic positive response of SOC to ΔNPP in the topsoil regardless of CNR (Fig. 1). However, the negative effect of CNR in the topsoil is still reflected by the nonlinearity of the responses in the topsoil (Fig. 1). To further distinguish the effect of CNR, we classified the soil profiles into two groups with contrasting vertical distributions of CNR along the soil profile: lower CNR in the topsoil versus lower CNR in the subsoil. Using ΔSOC estimates in the two groups, we fitted meta-regression

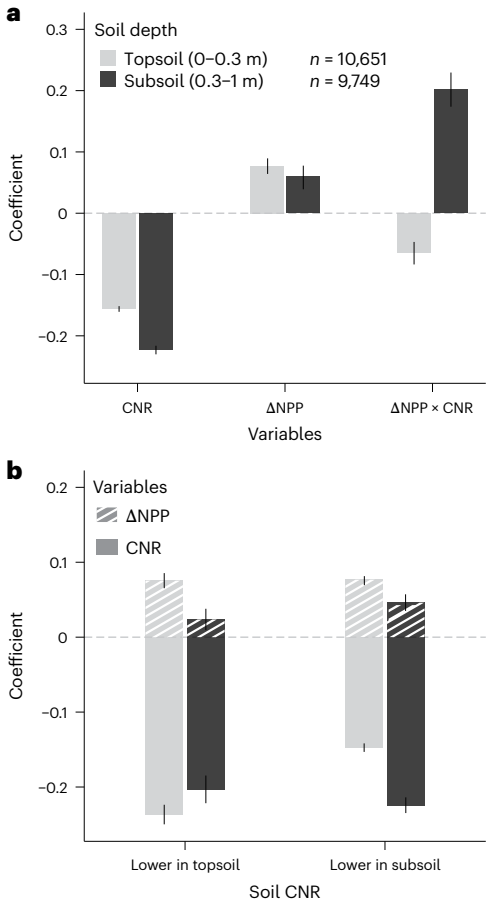

Fig. 3 | The effects of soil CNR and productivity changes on the response of SOC. a, The effects (coefficients) of the productivity changes (ΔNPP), CNR and their interaction on SOC responses in two soil depth layers estimated by a mixed-effects model driven by the standardized values of the three variables. The coefficients for ΔNPP, CNR and their interaction are modelled to vary by soil depth. **b**, The effects of ΔNPP and CNR on layer-specific SOC response as impacted by the vertical gradient of CNR across the two soil layers. Two contrasting vertical distributions of CNR along the soil profile are considered: lower CNR in the topsoil versus lower CNR in the subsoil. For each gradient, a separate mixed-effects model is fitted driven by ΔNPP and CNR, allowing the coefficients for the two variables to vary by soil depth. The error bars represent 95% confidence interval in both panels. *n* is the sample size of data using the mixed-effect models, which is the same in **a** and **b**.

for each group to elucidate how the vertical CNR gradients influence the relationships of ΔSOC with ΔNPP and CNR in the two depth layers. The results demonstrate that the slope for the negative relationship between ΔSOC and CNR is consistently steeper in the layer with lower CNR (Fig. 3b). That is, the lower the CNR, the stronger the negative association of SOC changes with CNR, regardless of soil depth layers.

Global spatial pattern of SOC responses

We developed cross-validated random forest models (R^2 for validation is 0.81, 0.81 and 0.79 for the 0–0.3-m, 0.3–1-m and 0–1-m soil depth layers, respectively; Extended Data Fig. 5) across global terrestrial ecosystems at the resolution of 1 km, and estimated SOC changes attributed to a typical scenario of 20% NPP increase (ΔSOC_{NPP}) by calculating the difference between ΔSOC in response to 1.5 °C warming plus 20% NPP increase and to 1.5 °C warming alone in each 1-km grid (Methods).

Across the globe, in the 0–0.3-m topsoil, 20% NPP increases either offset or exacerbate warming-induced SOC losses, but offsetting is most common (Fig. 4a). Central Africa, South America and

https://doi.org/10.1038/s41561-025-01697-1

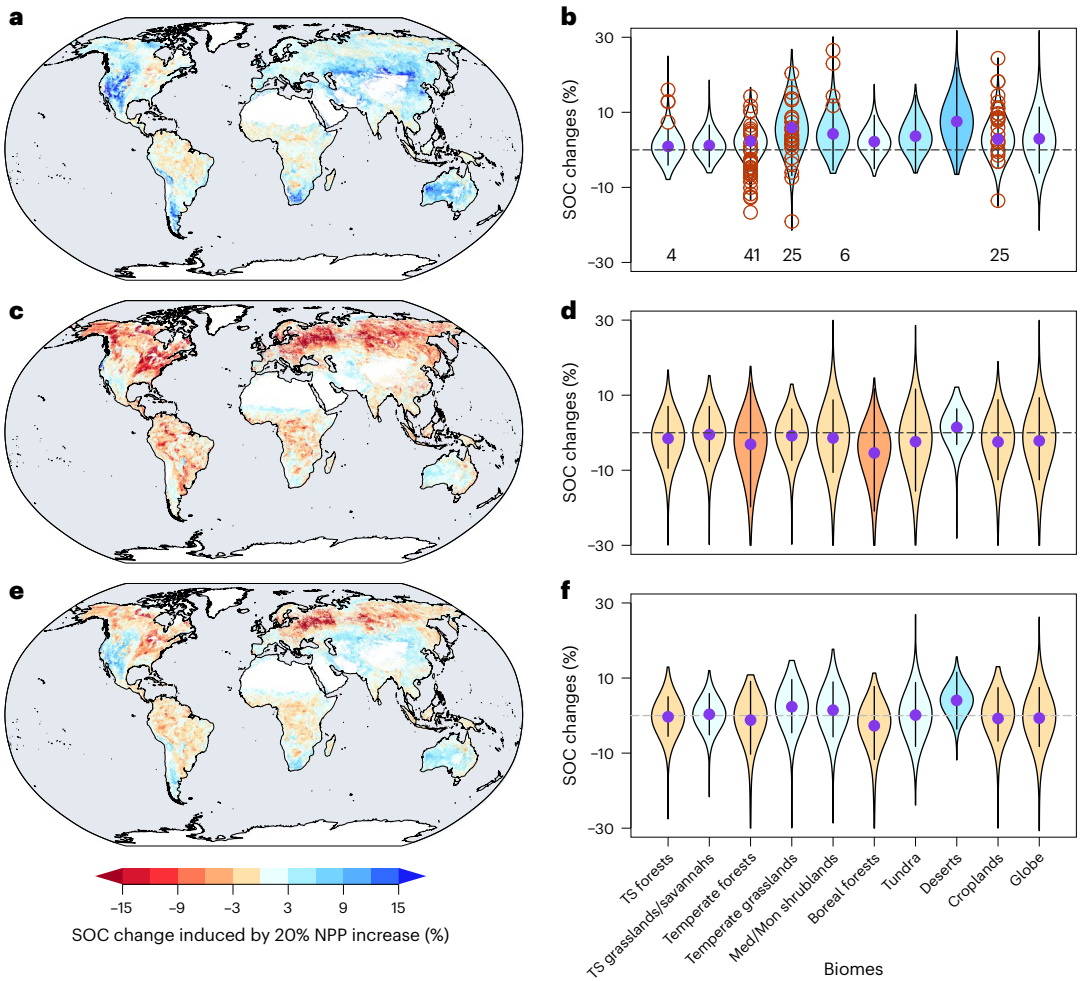

Fig. 4 | Global patterns of SOC changes attributed to plant productivity changes. The change is defined as the difference between responses of SOC to simultaneous 1.5 °C warming and a 20% plant productivity increase and that to 1.5 °C warming alone. This difference represents the additional changes in SOC induced by 20% plant productivity increases under warming. **a**,**b**, The global spatial pattern (**a**) and ecosystem-specific responses (**b**) in the 0–0.3-m topsoil. **c**,**d**, The global spatial pattern (**c**) and ecosystem-specific responses (**d**) in the 0.3–1-m subsoil. **e**,**f**, The global spatial pattern (**e**) and ecosystem-specific responses (**f**) in the 0–1-m profile. The red circles in **b** are the SOC changes observed in field experiments involving elevated CO_2 in the relevant ecosystems, which are adopted from ref. 12, and the numbers in **b** are the sample size of experimental data in the corresponding biomes. The purple points denote the mean SOC change for each ecosystem, with error bars representing one standard deviation. A map depicting uncertainties associated with the SOC changes is provided in Supplementary Fig. 4. The violin plots in **b**,**d**,**f** show the distribution of SOC change in **a**,**c**,**e** among biomes. Coastline data in **a**,**c**,**e** from Natural Earth (https://www.naturalearthdata.com/downloads/50m-physical-vectors/50m-coastline).

Southeast Asia are the main regions with exacerbated SOC losses. On average across the globe, percentage SOC losses induced by warming are decreased by 3.0 ± 0.3%, and this average offsetting occurs in all ecosystems (Fig. 4b and Supplementary Table 2). We compared the variation in predicted SOC changes in the topsoil with those observed in field experiments involving elevated CO_2, which usually enhances NPP[12]. The results indicate that the variance of predicted SOC changes is comparable to that observed in field experiments in the corresponding ecosystems (Fig. 4b).

In the 0.3–1-m subsoil, the majority of global terrestrial regions show exacerbated SOC losses, except in some dry regions, such as central Asia and central Australia (Fig. 4c). Averaging across the globe, the estimated additional average loss is 2.8 ± 0.5% (Fig. 4d and Supplementary Table 2). Taking the two depth layers together, 20% NPP increase results in an additional 15.7 ± 2.8 Pg SOC losses in the 0–1-m soil profile across the globe (Fig. 4f and Supplementary Table 2). On average, deserts are the ecosystem with the strongest positive effect of NPP increase on SOC, followed by temperate grasslands, Mediterranean/montane shrublands and tundra (Fig. 4f and Supplementary Table 2).

A nitrogen-driven framework

Given the leading importance of CNR for explaining SOC responses to NPP changes across soil depths, we propose a nitrogen-driven framework that interconnects additional plant growth and the relevant nitrogen (N) requirement to predict soil carbon (C) balance under warming and plant productivity changes (Fig. 5). Increased plant productivity enhances C inputs into the soil (especially the topsoil due to above-ground contributions and much denser roots compared to the subsoil), at least partially offsetting warming-induced C losses. However, additional plant growth requires additional N if assuming stoichiometric homoeostasis of plants[33]. This additional N demand may be met by the additional N mineralization induced by warming-accelerated C mineralization[6,15]. If not and assuming no changes in other N input sources, any remaining N deficit has to be filled by mining N from soil organic matter via priming, concomitant with the acceleration of C loss[34,35].

Hence, soil CNR is critical (Fig. 2), as low CNR soil layers release more N than high CNR soil layers per unit decomposition of soil C in the same soil profile. This can be attributed to a higher 'return on investment' in mining lower CNR soil organic matter[36–38], thereby intensifying

https://doi.org/10.1038/s41561-025-01697-1

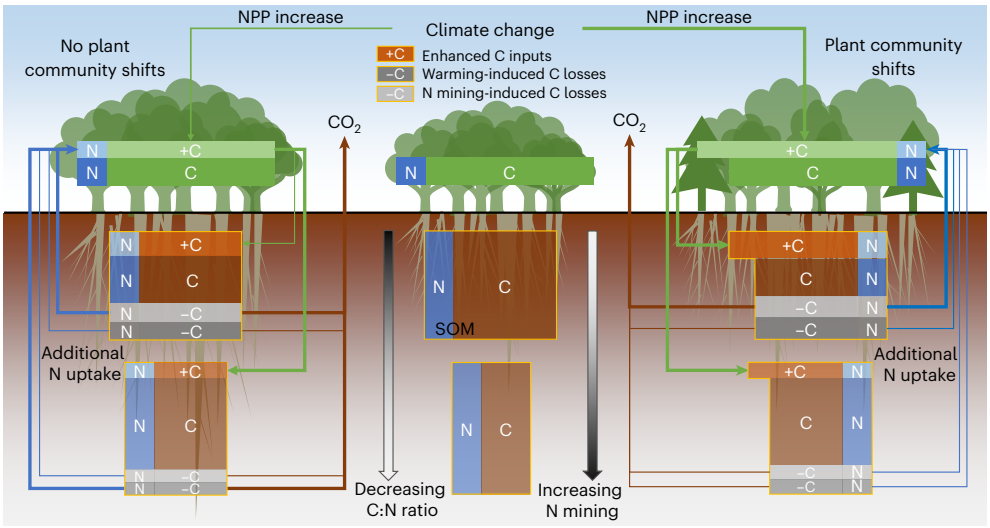

Fig. 5 | A nitrogen-driven framework for predicting SOC dynamics in response to warming and plant productivity increase. The final balance of SOC under warming and plant productivity alterations is governed by the allocation of N between plants and soil organic matter, further regulated by potential stoichiometric shifts of both components. Increased plant growth requires additional nitrogen (N) to maintain its stoichiometric balance (assuming no stoichiometric shifts). Under the assumption of no external N inputs, this extra N can come from: (1) warming-enhanced decomposition, which accelerates the breakdown of existing SOC, releases N; (2) N mining (if enough N is not released from decomposition), which results in plants to mine N from existing soil organic matter, further accelerating carbon loss. Soil CNR along the soil profile plays a key role. Soils (layers) with lower CNR (for example, subsoil) will release more N per unit of decomposed soil organic matter compared to high CNR soils (layers, for example, topsoil). This influences the extent of N mining needed to meet plant N demand. Plant communities may also shift, affecting the amount and quality of plant litter entering the soil and potentially changing their N acquisition strategies. The width of the arrows indicates the relative magnitude of the C and N flow.

SOC losses in soil layers with lower CNR like in the subsoil (Fig. 3). Across soil depths, subsoil indeed exhibits significantly lower CNR than topsoil on the global scale (Extended Data Fig. 6). It is also supported by the fact that if the topsoil has lower CNR than the subsoil, the relationship between ΔSOC and CNR has a steeper negative slope in the topsoil and vice versa (Fig. 3b). These results imply preferential N mining from soil layers with lower CNR. Supportively, more below-ground NPP is allocated to the subsoil as shown in Extended Data Fig. 3. Field experiments using ^{15}N tracers had also revealed that plant species with root traits (for example, deeper rooting depth) of effectively acquiring N from subsoil layers outcompete plants with shallower rooting depth under warming and elevated CO_2 conditions[39,40]. Such depth-specific N uptake behaviour of different plants may drive both short- and long-term shifts in subsoil biogeochemistry under climate change, influencing SOC dynamics across soil layers. Although N in deep soil layers may serve as a crucial N source for plants under climate change conditions[41,42], we have to note that subsoil C–N coupling processes in situ are poorly understood and more studies are required.

Under certain conditions, plant community composition may shift to alleviate N constraints[43,44]. Our assessment indicates that such shifts occur more frequently under higher absolute NPP changes (Methods and Extended Data Fig. 7), probably in response to N deficits. Changes in species composition and biomass stoichiometry (for example, C:N ratio) could alter N acquisition strategies, further influencing SOC dynamics (Fig. 5). This trade-off between C accumulation and N mining-induced SOC losses underpins the nonlinear SOC responses observed (Fig. 1a). Specifically, at moderate NPP increase (for example, 30% in this study), N mining outpaces the benefits of enhanced C inputs, leading to net SOC losses. As NPP continues to rise and crosses a tipping point (for example, exceeding 30%), plant community shifts and adaptation strategies may slow the acceleration of N mining, allowing C accumulation to outweigh losses, ultimately leading to net SOC gains.

We observe diverse SOC responses to warming and plant productivity changes in terms of both magnitude and direction at both the ecosystem level and globally and across soil depths. Multiple lines of evidence suggest that these diverse responses are fundamentally governed by soil N availability. If warming-induced N mineralization can meet plant demands, increased NPP may offset SOC losses. If not, plants intensify N mining, exacerbating SOC losses. The magnitude of the N deficit, along with the capacity of certain plant species (for example, N-fixing legumes) to acquire N, influences the response of plant communities[37,38]. In N-limited systems, plant communities may undergo shifts characterized by changes in biomass stoichiometry[5,45] or adaptations to enhance N mining efficiency[46,47]. Thus, the balance of SOC under warming and plant productivity alterations is governed by the allocation of N between plants and soil organic matter, further regulated by potential stoichiometric shifts of both components (Fig. 5).

The nitrogen-driven framework provides a foundation for understanding whole-profile SOC dynamics in response to warming and plant productivity changes and other global change factors. Nitrogen deposition and fertilizer application, for example, provide additional N to meet the requirements for additional plant growth and/or alleviate N mining, benefiting SOC accrual, particularly in N-limited systems[48,49]. In addition, plant community shifts involving N-fixing legumes may alleviate N scarcity, reducing reliance on N mining and benefiting carbon accrual. As soil organic matter also includes other nutrients (for example, phosphorous), the framework can be extrapolated to systems with plant growth limited by those nutrients. To improve predictions of SOC dynamics in response to warming and productivity changes, we emphasize that it is imperative to consider their interplay, which is ecosystem and soil layer specific and mediated by the availability of N and other nutrients. Boosting plant productivity is not enough for mitigating warming-induced SOC losses, particularly for deeper soil layers or nutrient-limited ecosystems and could even exacerbate SOC losses under climate change due to nutrient mining.

Online content

Any methods, additional references, Nature Portfolio reporting summaries, source data, extended data, supplementary information, acknowledgements, peer review information; details of author contributions and competing interests; and statements of data and code availability are available at https://doi.org/10.1038/s41561-025-01697-1.

References

1. Friedlingstein, P. et al. Global carbon budget 2023. *Earth Syst. Sci. Data* **15**, 5301–5369 (2023).
2. Davidson, E. A. & Janssens, I. A. Temperature sensitivity of soil carbon decomposition and feedbacks to climate change. *Nature* **440**, 165–173 (2006).
3. Crowther, T. W. et al. Quantifying global soil carbon losses in response to warming. *Nature* **540**, 104–108 (2016).
4. Wang, M. M. et al. Global soil profiles indicate depth-dependent soil carbon losses under a warmer climate. *Nat. Commun.* **13**, 5514 (2022).
5. Cui, J. et al. Elevated CO_2 levels promote both carbon and nitrogen cycling in global forests. *Nat. Clim. Change* **14**, 511–517 (2024).
6. Lie, Z. et al. Warming leads to more closed nitrogen cycling in nitrogen-rich tropical forests. *Glob. Chang. Biol.* **27**, 664–674 (2020).
7. Varney, R. M. et al. Simulated responses of soil carbon to climate change in CMIP6 Earth system models: the role of false priming. *Biogeosciences* **20**, 3767–3790 (2023).
8. Van Sundert, K. et al. When things get MESI: the Manipulation Experiments Synthesis Initiative—a coordinated effort to synthesize terrestrial global change experiments. *Glob. Chang. Biol.* **29**, 1922–1938 (2023).
9. Keenan, T. F. et al. A constraint on historic growth in global photosynthesis due to rising CO_2. *Nat. Clim. Change* **13**, 1376–1381 (2023).
10. Fernández-Martínez, M. et al. Global trends in carbon sinks and their relationships with CO_2 and temperature. *Nat. Clim. Change* **9**, 73–79 (2018).
11. Schimel, D., Stephens, B. B. & Fisher, J. B. Effect of increasing CO_2 on the terrestrial carbon cycle. *Proc. Natl Acad. Sci. USA* **112**, 436–441 (2014).
12. Terrer, C. et al. A trade-off between plant and soil carbon storage under elevated CO_2. *Nature* **591**, 599–603 (2021).
13. Xu, S. et al. Positive soil priming effects are the rule at a global scale. *Glob. Chang. Biol.* **30**, e17502 (2024).
14. Niu, S., Song, L., Wang, J., Luo, Y. & Yu, G. Dynamic carbon-nitrogen coupling under global change. *Sci. China Life Sci.* **66**, 771–782 (2023).
15. Butler, S. M. et al. Soil warming alters nitrogen cycling in a New England forest: implications for ecosystem function and structure. *Oecologia* **168**, 819–828 (2011).
16. Du, E. et al. Global patterns of terrestrial nitrogen and phosphorus limitation. *Nat. Geosci.* **13**, 221–226 (2020).
17. Pendall, E., Osanai, Y., Williams, A. L. & Hovenden, M. J. Soil carbon storage under simulated climate change is mediated by plant functional type. *Glob. Chang. Biol.* **17**, 505–514 (2011).
18. Carrillo, Y., Dijkstra, F., LeCain, D., Blumenthal, D. & Pendall, E. Elevated CO_2 and warming cause interactive effects on soil carbon and shifts in carbon use by bacteria. *Ecol. Lett.* **21**, 1639–1648 (2018).
19. Hartmann, H., Bahn, M., Carbone, M. & Richardson, A. D. Plant carbon allocation in a changing world—challenges and progress: introduction to a Virtual Issue on carbon allocation Introduction to a virtual issue on carbon allocation. *N. Phytol.* **227**, 981–988 (2020).
20. Mueller, K. E. et al. Root responses to elevated CO_2, warming and irrigation in a semi-arid grassland: integrating biomass, length and life span in a 5-year field experiment. *J. Ecol.* **106**, 2176–2189 (2018).
21. Hicks Pries, C. E. et al. The deep soil organic carbon response to global change. *Annu. Rev. Ecol. Evol. Syst.* **54**, 375–401 (2023).
22. He, Y. et al. Radiocarbon constraints imply reduced carbon uptake by soils during the 21st century. *Science* **353**, 1419–1424 (2016).
23. Xiao, L. J. et al. Younger carbon dominates global soil carbon efflux. *Glob. Chang. Biol.* **28**, 5587–5599 (2022).
24. Batjes, N. H., Calisto, L. & de Sousa, L. M. Providing quality-assessed and standardised soil data to support global mapping and modelling (WoSIS snapshot 2023). *Earth Syst. Sci. Data* **16**, 4735–4765 (2024).
25. Running, S., Mu, Q. & Zhao, M. *MOD17A3H MODIS/Terra Net Primary Production Yearly L4 Global 500m SIN Grid V006* (NASA EOSDIS Land Processes Distributed Active Archive Center, 2015).
26. Xiao, L. J. et al. Global depth distribution of belowground net primary productivity and its drivers. *Glob. Ecol. Biogeogr.* **32**, 1435–1451 (2023).
27. Wieder, W. R., Cleveland, C. C., Smith, W. K. & Todd-Brown, K. Future productivity and carbon storage limited by terrestrial nutrient availability. *Nat. Geosci.* **8**, 441–444 (2015).
28. Smith, W. K. et al. Large divergence of satellite and Earth system model estimates of global terrestrial CO_2 fertilization. *Nat. Clim. Change* **6**, 306–310 (2016).
29. Li, P. et al. Quantification of the response of global terrestrial net primary production to multifactor global change. *Ecol. Indic.* **76**, 245–255 (2017).
30. Hu, Q. & Feng, S. A daily soil temperature dataset and soil temperature climatology of the contiguous United States. *J. Appl. Meteorol. Climatol.* **42**, 1139–1156 (2003).
31. Song, J. et al. A meta-analysis of 1,119 manipulative experiments on terrestrial carbon-cycling responses to global change. *Nat. Ecol. Evol.* **3**, 1309–1320 (2019).
32. Liu, S. et al. Climatic role of terrestrial ecosystem under elevated CO_2: a bottom-up greenhouse gases budget. *Ecol. Lett.* **21**, 1108–1118 (2018).
33. Elser, J. J., Fagan, W. F., Kerkhoff, A. J., Swenson, N. G. & Enquist, B. J. Biological stoichiometry of plant production: metabolism, scaling and ecological response to global change. *N. Phytol.* **186**, 593–608 (2010).
34. Wen, Z., White, P. J., Shen, J. & Lambers, H. Linking root exudation to belowground economic traits for resource acquisition. *N. Phytol.* **233**, 1620–1635 (2021).
35. Macdonald, C. A., Delgado-Baquerizo, M., Reay, D. S., Hicks, L. C. & Singh, B. K. in *Soil Carbon Storage* (ed. Singh, B. K.) 167–205 (Academic Press, 2018).
36. Dijkstra, F. A., Carrillo, Y., Pendall, E. & Morgan, J. A. Rhizosphere priming: a nutrient perspective. *Front. Microbiol.* **4**, 126 (2013).
37. Terrer, C., Vicca, S., Hungate, A. B., Phillips, R. P. & Prentice, I. C. Mycorrhizal association as a primary control of the CO_2 fertilization effect. *Science* **353**, 72–74 (2016).
38. Terrer, C. et al. Ecosystem responses to elevated CO_2 governed by plant-soil interactions and the cost of nitrogen acquisition. *N. Phytol.* **217**, 507–522 (2018).
39. Pedersen, E. P., Elberling, B. & Michelsen, A. Foraging deeply: depth-specific plant nitrogen uptake in response to climate-induced N-release and permafrost thaw in the High Arctic. *Glob. Chang. Biol.* **26**, 6523–6536 (2020).
40. McKinley, D. C., Romero, J. C., Hungate, B. A., Drake, B. G. & Megonigal, J. P. Does deep soil N availability sustain long-term ecosystem responses to elevated CO_2? *Glob. Chang. Biol.* **15**, 2035–2048 (2009).
41. Nakayama, M. et al. Quantitative importance of subsoil nitrogen cycling processes in Andosols and Cambisols under temperate forests. *Appl. Soil Ecol.* **201**, 105485 (2024).
42. Odone, A., Popovic, O. & Thorup-Kristensen, K. Deep roots: implications for nitrogen uptake and drought tolerance among winter wheat cultivars. *Plant Soil* **500**, 13–32 (2023).

43. Zelikova, T. J. et al. Long-term exposure to elevated CO_2 enhances plant community stability by suppressing dominant plant species in a mixed-grass prairie. *Proc. Natl Acad. Sci. USA* **111**, 15456–15461 (2014).
44. Langley, J. A. & Megonigal, J. P. Ecosystem response to elevated CO_2 levels limited by nitrogen-induced plant species shift. *Nature* **466**, 96–99 (2010).
45. Cotrufo, M. F., Ineson, P. & Scott, A. Elevated CO_2 reduces the nitrogen concentration of plant tissues. *Glob. Chang. Biol.* **4**, 43–54 (2002).
46. Xu, Q., Wang, X. & Tang, C. The effects of elevated CO_2 and nitrogen availability on rhizosphere priming of soil organic matter under wheat and white lupin. *Plant Soil* **425**, 375–387 (2018).
47. Pausch, J., Holz, M., Zhu, B. & Cheng, W. Rhizosphere priming promotes plant nitrogen acquisition by microbial necromass recycling. *Plant Cell Environ.* **47**, 1987–1996 (2024).
48. Tang, B., Rocci, K. S., Lehmann, A. & Rillig, M. C. Nitrogen increases soil organic carbon accrual and alters its functionality. *Glob. Chang. Biol.* **29**, 1971–1983 (2023).
49. Hu, Y. et al. Depth-dependent responses of soil organic carbon under nitrogen deposition. *Glob. Chang. Biol.* **30**, e17247 (2024).

[1]State Key Laboratory of Soil Pollution Control and Safety, College of Environmental and Resource Sciences, Zhejiang University, Hangzhou, China. [2]Key Laboratory of Environment Remediation and Ecological Health, Ministry of Education, Zhejiang University, Hangzhou, China. [3]Faculty of Geographical Science, Beijing Normal University, Beijing, China. [4]College of Agriculture, Nanjing Agricultural University, Nanjing, China. [5]Key Laboratory of Vegetation Restoration and Management of Degraded Ecosystems, South China Botanical Garden, Chinese Academy of Sciences, Guangzhou, China. [6]Key Laboratory of Ecosystem Network Observation and Modelling, Institute of Geographic Sciences and Natural Resources Research, Chinese Academy of Sciences, Beijing, China. [7]State Key Laboratory of Vegetation and Environmental Change, Institute of Botany, Chinese Academy of Sciences, Beijing, China. [8]School of Integrative Plant Science, Cornell University, Ithaca, NY, USA. [9]Nanjing Institute of Geography and Limnology, Chinese Academy of Sciences, Nanjing, China. ✉e-mail: luozk@zju.edu.cn

Methods

Soil profiles

We used the latest global soil profile database (the 2023 snapshot) collated and managed by the World Soil Information Service[24], which has been quality controlled using standardized processes. To ease comparison and analysis, we further harmonized soil organic carbon content (SOC_c, g C kg^{-1} soil) into two standard depths (that is, 0–0.3- and 0.3–1-m soil layers) using mass-preserving splines[50]. At last, we obtained 121,345 and 92,193 SOC_c measurements in the 0–0.3- and 0.3–1-m soil depth, respectively. Using the SOC_c measurements, SOC stock (SOC_s, Mg C ha^{-1}) in the two depth layers were further calculated combining estimates of soil bulk density and gravel content as described in ref. 51. The SOC_s in the 0–1 m is calculated as the sum of SOC_s in the 0–0.3- and 0.3–1-m depth layers. Another 2,778 measurements in the three depth layers from permafrost-affected regions[52] were also included in the dataset.

From the same database and using the same approach, total soil nitrogen content (TN_c) and stock (TN_s) was obtained for the three standard layers. About 5% soil profiles do not have nitrogen records. To amplify the use of SOC measurements, missing nitrogen data were extracted from WISE (World Inventory of Soil Emission Potentials)[53]. The soil carbon-to-nitrogen mass ratio (CNR) in each soil layer was then calculated. Finally, we obtained 124,123; 94,971 and 94,971 data points including SOCs, TNs and CNR for three standard soil layers, respectively (Extended Data Fig. 1). The locations of the soil profiles span across global terrestrial ecosystems, covering all major biome groups with mean annual temperature ranging from −20.0 to 30.7 °C and mean annual precipitation from 0 to 6,674 mm.

Net primary productivity and its allocation

We used two observational global datasets of NPP derived from satellite images and field survey, respectively. The satellite-derived NPP product was generated by remote sensing observations of the moderate-resolution imaging spectroradiometer (MODIS) with a 1-km spatial resolution[54]. It is one of the most widely used NPP products and contains annual NPP estimates in each 1-km grid during the period 2001–2022. In the grid with soil profiles, we calculated the grid-level average NPP from 2001 to 2022 to represent the average NPP at the location of each individual soil profile (that is, soil profiles in the same grid share the same NPP).

The field-observation-derived NPP dataset is a global mapping product at 1-km spatial resolution[23]. Briefly, a global dataset including field NPP from 725 soil profiles, root biomass and its depth distribution from 559 soil profiles were compiled and used to train a machine-learning-based model to infer the depth distribution of below-ground NPP (BNPP) across the globe and digitally map depth-resolved BNPP globally at 1-km resolution. The depth allocation of BNPP was assumed to follow the depth distribution of root biomass and turnover, with the consideration of vertical carbon transport along the soil profile induced by leaching and/or bioturbation using a partial differential equation[26,55]. A detailed description of the BNPP dataset and the modelling for the depth allocation of BNPP can be found in ref. 26. From this mapping product, NPP, BNPP and its fractional allocation to different soil depth layers (f_{BNPP}) at the location of each soil profile were extracted to represent the above- and below-ground allocation of NPP and its vertical allocation in each soil profile. The MODIS NPP and observation-derived NPP were averaged to represent the average NPP at each location.

Environmental covariates

Mean annual temperature (MAT) and precipitation (MAP) at each soil profile location were extracted from WorldClim version 2 (ref. 56), which is a global mapping product at the resolution of 0.0083° × 0.0083° using monthly temperature and precipitation records during the period 1970–2000. Soil profiles in the same 0.0083° grid (that is, ~1 km^2 at the equator) share the same MAT and MAP. The WWF (World Wildlife Fund) map of terrestrial ecoregions of the world[57] was used to extract the biome type at each soil profile. The MODIS land-cover map[58] at the same resolution of WorldClim was used to identify whether the soil profile was located in a cultivated land (that is, cropland or cropland/natural vegetation mosaic). A global landform spatial layer was obtained from Global Landform Classification[59] to identify the landform at each soil location. Global terrestrial lands were divided into three general landform types: plains including lowlands, plateaus and mountains including hills. A global spatial map of the 12 United States Department of Agriculture soil orders was used to distinguish the soil type at each soil profile. The dominant mycorrhizal type at each soil profile location was gained from the global map of the percentage of above-ground plant biomass of mycorrhizal vegetation[60]. A detailed list of the environmental covariates was presented and described in Supplementary Table 1.

Space-for-change substitution

The more than 120,000 soil profiles cover diverse climatic and edaphic conditions across the globe. We used a modified space-for-change substitution combined with meta-analysis techniques to quantify the response of SOC to NPP changes and warming under various environmental conditions[4]. The approach has been explicitly described in ref. 4 and applied to estimate the responses of whole-soil profile SOC to warming[4] and climate extremes[61]. Taking advantage of the global spatial coverage of the dataset (Extended Data Fig. 1), the approach controls other confounding variables such as soil type and landform and precipitation and its seasonality and disentangles their influence. Using the approach, we quantified the responses of SOC to a series of scenarios of plant productivity changes under warming (Extended Data Fig. 2). To cover potential changes in NPP under climate change, a gradient of NPP changes from −20% to 60% by 10% increment was considered, whereas the warming magnitude was assigned to 1.5 °C, which is the internationally agreed warming limit[62].

In detail, a soil profile was first randomly selected from the 124,123 soil profiles. This profile was treated as a criterion to select a group of soil profiles sharing the same MAT, MAP, precipitation seasonality, landform and soil type. This group is called ambient group (A group; Extended Data Fig. 2). Then, another two groups (that is, W and W+NPP groups; Extended Data Fig. 2) were selected according to the same selection criterion defined by the A group except MAT and NPP. Specifically, the MAT in W group must be certain degrees higher (1.5 °C in this study) than that in the A group to reflect warming. Similarly, the MAT and average NPP in W+NPP groups must be certain degrees higher than that in the A group to represent simultaneous warming and NPP changes (that is, ΔNPP, the changes scenarios from −20% to 60% by 10% interval). During the selection process, as MAT, NPP and MAP are continuous variables, they cannot be exactly the same in the same group and so tolerance values (τ, which defines the allowed maximum deviation of MAT, NPP and MAP in the same group) of 0.5 °C, 5%, and 25 mm were assigned for MAT, NPP and MAP, respectively[4].

By conducting the above selection and grouping processes, we obtained a triple including three groups (that is, a set of A, W and W+NPP). With the replacement of sampled profiles, the random selection of the criterion profile and grouping processes were repeated to gain enough triples, and the selected criterion profile must be unique and has not been selected as the criterion profile in any triples. Additionally, triples that include groups with one soil profile were excluded. At last, we obtained a set of triples with the same warming and NPP change levels under different baseline environmental conditions (that is, ambient MAT, MAP, precipitation seasonality, soil type and landform). Within triples, as the groups share the same environmental conditions, the effects of those environmental covariates are thus eliminated, facilitating the quantification of SOC changes as impacted by warming and NPP. Whereas the effects of those

environmental covariates are reflected by the difference of SOC responses among triples.

Here we would like to note that all soil profiles in the same A group belong to the same biome, but biome type is allowed to change in the corresponding W and W+NPP groups as warming and NPP changes may be associated with plant community shifts. Other environmental factors, such as soil nitrogen and pH, are not controlled in the grouping process. The main reason is that these biophysical factors may shift with warming/NPP changes[63]. The selection itself will determine this shift, which can be reflected by the difference of these factors between the A and W/W+NPP groups. So the difference of SOC among triples reflect the long-term, integrated effects of warming/NPP changes on SOC via potential direct and/or indirect pathways (for example, warming-induced shifts in vegetation and soil properties).

Estimation of the response of SOC to warming and NPP changes

Meta-analysis techniques were used to estimate the response of SOC to W+NPP by comparing SOC stock in the A group to that in the W+NPP groups, respectively. For the *i*th selected triple (A, W and W+NPP), the logarithmic response ratios of SOC ($\ln R_i$) to W and W+NPP could be calculated, respectively, as:

$$\ln R_{W,i} = \ln\left(\frac{\overline{SOC_{W,i}}}{\overline{SOC_{A,i}}}\right), \quad (1)$$

$$\ln R_{W+NPP,i} = \ln\left(\frac{\overline{SOC_{W+NPP,i}}}{\overline{SOC_{A,i}}}\right), \quad (2)$$

where $\overline{SOC_{A,i}}$, $\overline{SOC_{W,i}}$ and $\overline{SOC_{W+NPP,i}}$ are the mean SOC stock in the A, W and W+NPP groups of the *i*th triples, respectively.

Then the individual $\ln R_{W+NPP,i}$ values calculated for each triple were used to estimate a global mean response ratio ($\overline{\ln R_{W+NPP}}$) by a weighted mixed-effects model using the *rma.av* function in metafor in R version 4.1.1. The weight (w) was calculated as the inverse of the sum of within- (v) and between-group (τ^2) variances in the same triple:

$$\overline{\ln R_{W+NPP}} = \frac{\sum(\ln R_{W+NPP,i} \times w_i)}{\sum w_i}, \quad (3)$$

where $w_i = \frac{1}{v_i+\tau^2}$ is the weight for the $\ln R_{W+NPP,i}$ in the *i*th triple. The within-group variance (v) was calculated as:

$$v_i = \frac{S^2_{W+NPP}}{N_{W+NPP}X^2_{W+NPP}} + \frac{S^2_A}{N_A X^2_A}, \quad (4)$$

where S_{W+NPP} and S_A are the standard deviation of SOC in the W+NPP (or W) and A groups, respectively; X_{W+NPP} and X_A are the mean of SOC in the W+NPP (or W) and A groups, respectively; N_{W+NPP} and N_A are the number of samples (that is, the number of soil profiles) in the W+NPP (or W) and A groups, respectively. The between-group variance (τ^2) was estimated by restricted maximum likelihood. To assist interpretation, $\overline{\ln R_{W+NPP}}$ were back transformed and reported as percentage change, that is, $\Delta SOC = (e^{\overline{\ln R_{W+NPP}}} - 1) \times 100\%$. The back-transformed values were also used for subsequent data analyses.

In addition to calculating the response ratio on the global scale, to evaluate potential differences in SOC responses among different ecosystems, the response ratios have also been estimated at the ecosystem level by including only triples with A groups sharing the same biome type. Here it should be noted that plant community change would be associated with warming and plant productivity changes. So soil profiles in the W and W+NPP groups would be different in terms of biome type (that is, plant community shift with climate change).

Robustness assessment

In addition to the controlled precipitation, precipitation seasonality, landform and soil type, the space-for-change substitution approach implicitly assumes[64] that other land surface processes (for example, land use, ecosystem successional stages) that may influence SOC dynamics are not systematically different among the three groups in the same triple[4,61]. For example, if the A group contains only profiles located in cultivated lands and the W+NPP group contains only profiles located in natural lands, the estimated SOC change would be predominantly induced by the difference in land use and management, potentially masking the effects of warming and plant productivity changes. To test the stability of the estimates of SOC change, we repeated the global-scale assessment by excluding soil profiles from croplands. The new estimates of SOC response were comparable with the original estimates including cropland soils (Supplementary Fig. 1). The two estimates in terms of both magnitude and trend were similar in both topsoil and subsoil (Supplementary Fig. 1). Additionally, to demonstrate the influence of these soil with relatively extreme CNR values, we compared the SOC responses estimated using all data to that using data excluding soil profiles with a CNR of <1 or >100 (Supplementary Fig. 2). No significant differences were observed between the two estimates. To check the reasonability of the spatial distribution of triples, the 2,000 triples randomly selected were shown in Supplementary Fig. 3, which reveals that nearly all triples have a relatively small space, further demonstrating the reasonability of the approach.

Driver analysis

To explore the variation in the response ratios of SOC (that is, $\ln R_{W+NPP,i}$) across the globe and elucidate its drivers, a machine-learning-based statistical model—random forest (RF)—was fitted. The model aimed to elucidate the role of climate conditions, soil properties, vegetation properties and terrain attributes, incorporating a total of 39 potential environmental variables (Supplementary Table 1). Before fitting the model, collinearity among the predictor variables was assessed using the variance inflation factor (VIF) with the *vif* function in the car package in R version 4.1.1. Predictors with a VIF greater than 10 (16 out of the 39 variables) were excluded from the analysis. A tenfold cross-validation approach was employed to optimize model hyperparameters, including mtry (number of randomly drawn candidate predictors), splitrule (splitting rule) and min.node.size (minimal node size), using the *train* function in the caret package. The best RF model was selected based on the highest coefficient of determination (R^2).

The relative importance of each predictor was estimated by permutation variable importance using the *varImp* function in R package caret. Briefly, based on the times a predictor selected for branch splitting when growing a tree in model, the mean square error for every given regression tree with out-of-bag estimates is calculated. The change of model residuals due to that splitting represents the influence of the predictor. To compare the relative importance of individual predictors, their influences were first normalized by the total influence of all predictors and then multiplied by the explanatory power of the model for variation (that is, R^2; Fig. 2a,b). In addition, using from all NPP change scenarios, a mixed-effect model treating soil CNR and NPP change (which are the two most important predictors of SOC changes; Fig. 2) as the fixed factors and the depth layers as the random factor. This model allows us to test whether and how the effects of CNR and NPP on SOC changes depend on soil depths. Using standardized values (that is, *z*-score) of CNR and NPP changes (as such, model coefficients can indicate relative importance of the effects of CNR, ΔNPP and their interactions), the mixed-effect model analysis was conducted by using the lmerTest package in R version 4.2.2.

Global mapping

To illustrate the global spatial pattern of ΔSOC as impacted by warming and plant productivity changes, the cross-validated RF model for

lnR_{W+NPP} (Extended Data Fig. 5) was applied under two specific scenarios: S1, 1.5 °C warming without NPP changes; S2, 1.5 °C warming plus 20% NPP increase. The 20% NPP increment was selected as a representative example, reflecting empirical observations and multi-model projections of NPP changes[27–29]. The model was synchronously applied under the two scenarios at the resolution of 1 km across the globe using gridded data of model predictors. Predictors that were not at the 1-km resolution were resampled to 1 km. The baseline SOC stock, together with other soil properties required by the model, used the WISE dataset[53]. For the predictor Δf_{BNPP}, we assumed that it is equal to 0. The additional SOC changes in each pixel induced by the 20% NPP increase was calculated as difference between SOC changes predicted under the S2 scenario and that under S1 scenario, resulting in 500 estimates of the additional changes by the 500 trees in the RF model. The uncertainty of this additional SOC changes was estimated as the standard error of the 500 estimates (Supplementary Fig. 4).

Data availability

The latest WoSIS dataset24 can be accessed at https://www.isric.org/news/wosis-new-set-standardized-soil-profiles-released-wosislatest-june-2022. The MODIS NPP data can be accessed at https://lpdaac.usgs.gov/products/mod17a3hgfv061/. The field-observation-derived NPP and its allocation in soil layers dataset can be gained from ref. 26. Other data used in this study are the same as those used in ref. 4, which are publicly accessible. The coastline data in all maps are publicly accessible and can be accessed at https://www.naturalearthdata.com/downloads/50m-physical-vectors/50m-coastline/. Source data are provided with this paper.

Code availability

Code (R scripts developed using R version 4.2.2) used to assess the data and generate the results are accessible via figshare at https://doi.org/10.6084/m9.figshare.25859092 (ref. 65).

References

50. Bishop, T. F. A., McBratney, A. B. & Laslett, G. M. Modelling soil attribute depth functions with equal-area quadratic smoothing splines. *Geoderma* **91**, 27–45 (1999).
51. Luo, Z. K., Viscarra-Rossel, R. A. & Qian, T. Similar importance of edaphic and climatic factors for controlling soil organic carbon stocks of the world. *Biogeosciences* **18**, 2063–2073 (2021).
52. Mishra, U. et al. Spatial heterogeneity and environmental predictors of permafrost region soil organic carbon stocks. *Sci. Adv.* **7**, eaaz5236 (2021).
53. Batjes, N. H. Harmonized soil property values for broad-scale modelling (WISE30sec) with estimates of global soil carbon stocks. *Geoderma* **269**, 61–68 (2016).
54. Zhao, M. S. & Running, S. W. Drought-induced reduction in global terrestrial net primary production from 2000 through 2009. *Science* **329**, 940–943 (2010).
55. Koven, C. D. et al. The effect of vertically resolved soil biogeochemistry and alternate soil C and N models on C dynamics of CLM4. *Biogeosciences* **10**, 7109–7131 (2013).
56. Fick, S. E. & Hijmans, R. J. WorldClim 2: new 1-km spatial resolution climate surfaces for global land areas. *Int. J. Climatol.* **37**, 4302–4315 (2017).
57. Olson, D. M. et al. Terrestrial ecoregions of the world: a new map of life on Earth. *BioScience* **51**, 933–938 (2001).
58. Channan, S., Collins, K. & Emanuel, W. *Global Mosaics of the Standard MODIS Land Cover Type Data* (Univ. of Maryland & Pacific Northwest National Laboratory, 2014).
59. Meybeck, M., Green, P. & Vörösmarty, C. A new typology for mountains and other relief classes: an application to global continental water resources and population distribution. *Mt. Res. Dev.* **21**, 34–45 (2001).
60. Soudzilovskaia, N. A. et al. Global mycorrhizal plant distribution linked to terrestrial carbon stocks. *Nat. Commun.* **10**, 5077 (2019).
61. Wang, M. et al. Responses of soil organic carbon to climate extremes under warming across global biomes. *Nat. Clim. Change* **14**, 98–105 (2023).
62. Allen, M., Mustafa, B. & Shukla, P. *Global Warming of 1.5 °C* (eds Masson-Delmotte, V. et al.) (Cambridge Univ. Press, 2018).
63. Maes, S. L. et al. Environmental drivers of increased ecosystem respiration in a warming tundra. *Nature* **629**, 105–113 (2024).
64. Strayer, D. et al. Long-term ecological studies: an illustrated account of their design, operation, and importance to ecology. *Adv. Ecol. Acad. Sin.* **5**, 51–55 (1988).
65. Wang, M. Increasing plant productivity exacerbates global soil carbon losses under a warmer climate due to nitrogen mining. *figshare* https://doi.org/10.6084/m9.figshare.25859092.v3 (2024).

Acknowledgements

This research has been financially supported by the National Natural Science Foundation of China (grant numbers 32241036, 32171639) and the Postdoctoral Fellowship Program and China Postdoctoral Science Foundation (grant number BX20240314).

Author contributions

Z.L. conceived the study; M.W. compiled the data with the contribution of G.W., L.X. and Z.L.; M.W. and Z.L. designed the approach and data assessment procedure; M.W. conducted the data assessment and wrote the first draft; Z.L. revised the paper with the contributions of all authors.

Competing interests

The authors declare no competing interests.

Additional information

Extended data is available for this paper at https://doi.org/10.1038/s41561-025-01697-1.

Supplementary information The online version contains supplementary material available at https://doi.org/10.1038/s41561-025-01697-1.

Correspondence and requests for materials should be addressed to Zhongkui Luo.

Peer review information *Nature Geoscience* thanks Ben Bond-Lamberty, Emanuele Lugato and the other, anonymous, reviewer(s) for their contribution to the peer review of this work. Primary Handling Editors: Xujia Jiang and Stefan Lachowycz, in collaboration with the *Nature Geoscience* team.

https://doi.org/10.1038/s41561-025-01697-1

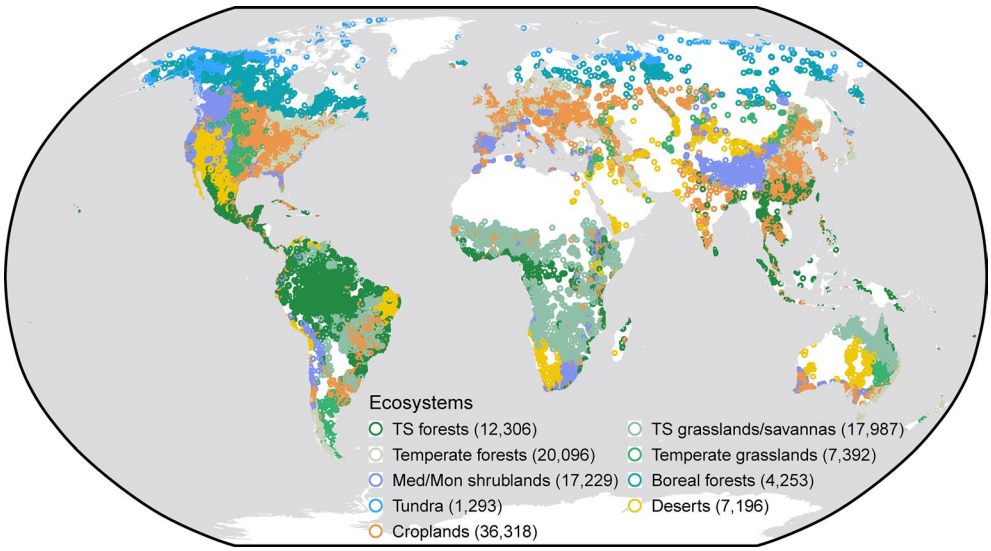

Extended Data Fig. 1 | The global distribution of soil profiles among biomes. The number behind biomes is the sample size of soil profiles in the biome. This data contains the latest WoSIS[24]. TS forests, tropical/subtropical forests; Med/Mon shrublands, Mediterranean/montane shrublands; TS grasslands/savannas, tropical/ subtropical grasslands/savannas. Coastline data from Natural Earth (https://www.naturalearthdata.com/downloads/50m-physical-vectors/50m-coastline).

https://doi.org/10.1038/s41561-025-01697-1

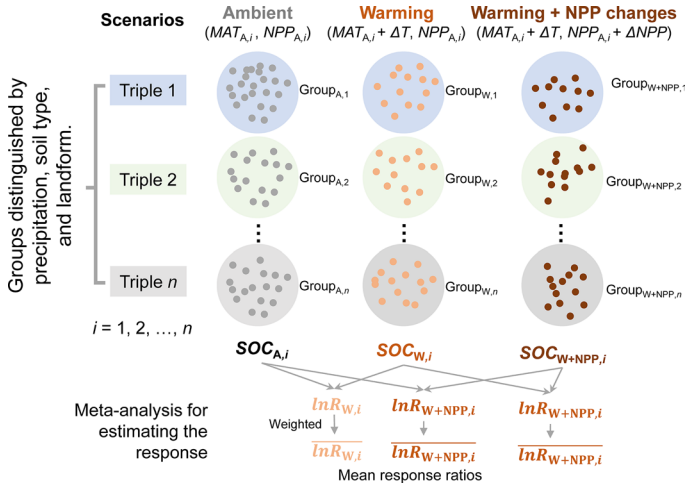

Extended Data Fig. 2 | Schematic representation of the approach used to quantify the response of soil organic carbon (SOC) to plant productivity changes and warming. Each dot represents one SOC observation. Dots in the i^{th} plate share the same mean annual temperature ($MAT_{A,i}$) and plant productivity ($NPP_{A,i}$), while dots in the same color plates indicate a group sharing the same mean annual precipitation (*MAP*), precipitation seasonality, landform, and soil type. ΔNPP (shown in Supplementary Table 1) and ΔT (1.5 °C in this study) are changes in NPP_A and MAT_A of interest, respectively. SOC values in the warming (W), and warming plus NPP changes (W+NPP) plates are compared to the values in the ambient (A) plates in the same group to calculate a weighted average effect size (i.e., the response of SOC to ΔT, and $\Delta T + \Delta NPP$) by the inverse of the sum of within- and between-group variances, using meta-analytic techniques (Methods). Figure adapted with permission from ref. 4, Springer Nature Limited.

https://doi.org/10.1038/s41561-025-01697-1

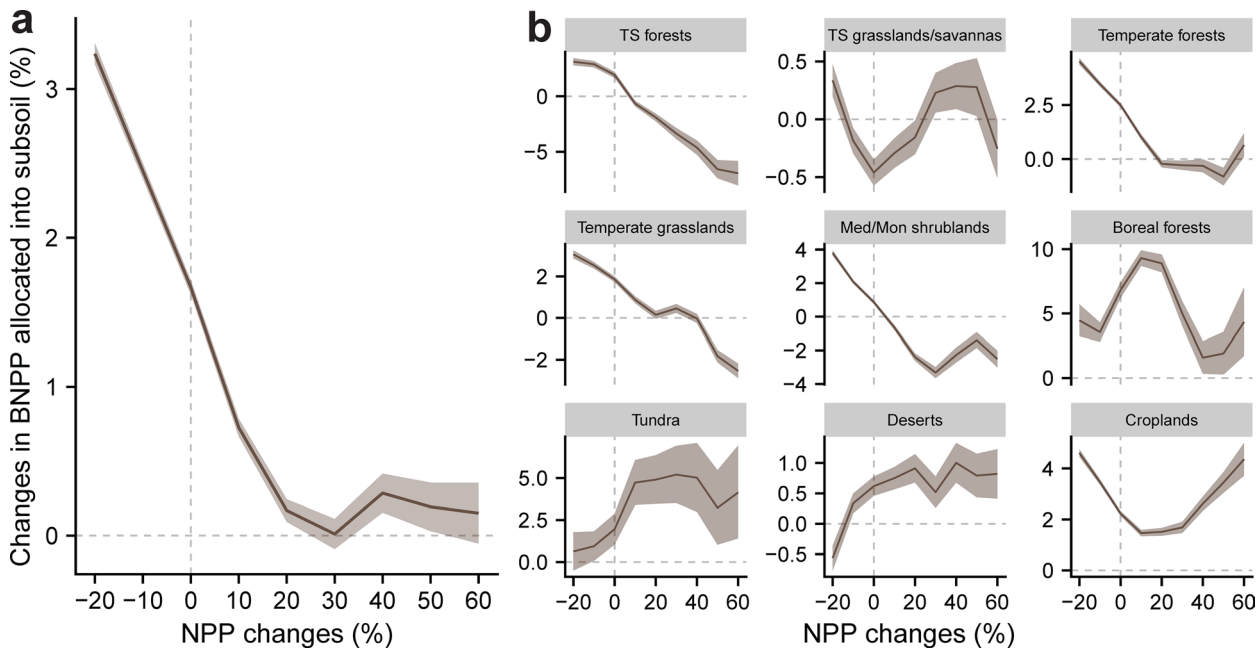

Extended Data Fig. 3 | Changes in belowground net primary productivity (BNPP) allocation. a, the changes [($BNPP_{0.3\text{-}1m}$/$BNPP_{\text{-Treatment}}$ − $BNPP_{0.3\text{-}1m}$/$BNPP_{\text{-Control}}$) / ($BNPP_{0.3\text{-}1m}$/$BNPP_{\text{-Control}}$)] in BNPP allocated into subsoil (0.3–1 m) on a global scale. **b**, the changes in BNPP allocated into subsoil among ecosystems. Dashed line shows the 1:1 line. The shading envelope represents the 95% confidence interval, with the corresponding similar colour solid line shows the average. TS forests, tropical/subtropical forests; Med/Mon shrublands, Mediterranean/montane shrublands; TS grasslands/savannas, tropical/ subtropical grasslands/savannas.

https://doi.org/10.1038/s41561-025-01697-1

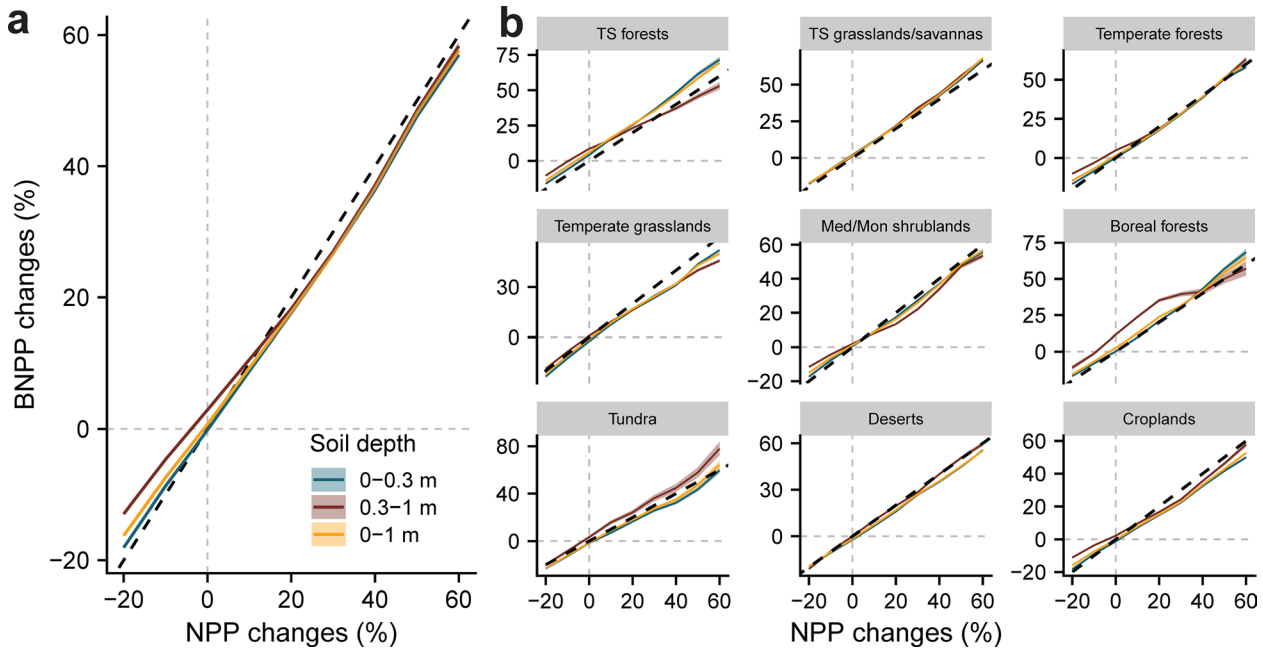

Extended Data Fig. 4 | Changes in belowground net primary productivity (BNPP) under warming and NPP change scenarios. a, BNPP changes coincide total NPP changes in all three soil depth layers on a global scale. **b**, BNPP changes in three soil depth layers among ecosystems. Dashed line shows the 1:1 line. The shading envelope represents the 95% confidence interval, with the corresponding similar colour solid line shows the average. TS forests, tropical/ subtropical forests; Med/Mon shrublands, Mediterranean/montane shrublands; TS grasslands/savannas, tropical/ subtropical grasslands/savannas.

https://doi.org/10.1038/s41561-025-01697-1

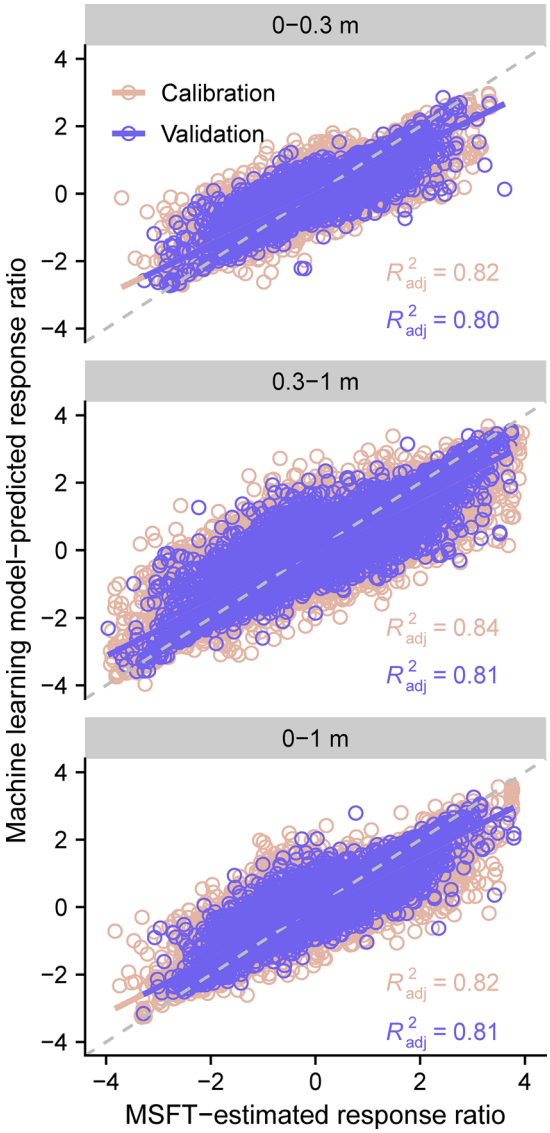

Extended Data Fig. 5 | The performance of random forest model for predicting global soil organic carbon changes induced by 20% NPP increase. The colour solid line is the regression line. The grey dotted line represents 1:1 line.

https://doi.org/10.1038/s41561-025-01697-1

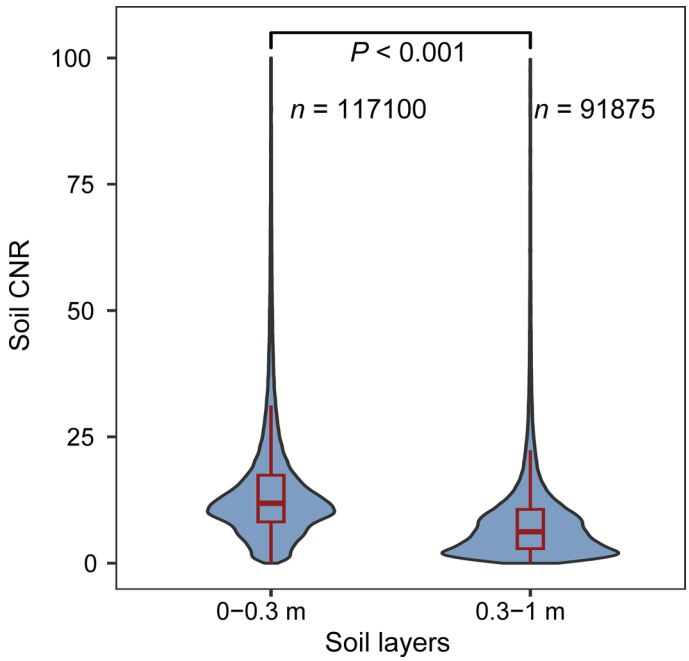

Extended Data Fig. 6 | The difference of soil carbon:nitrogen ratio between two soil depth layers. Boxplots show the median and interquartile range (IQR), with whiskers extending to the most extreme values within the 1.5 times of IQR. *n* represents the sample size. *P* values are for two-tailed tests.

https://doi.org/10.1038/s41561-025-01697-1

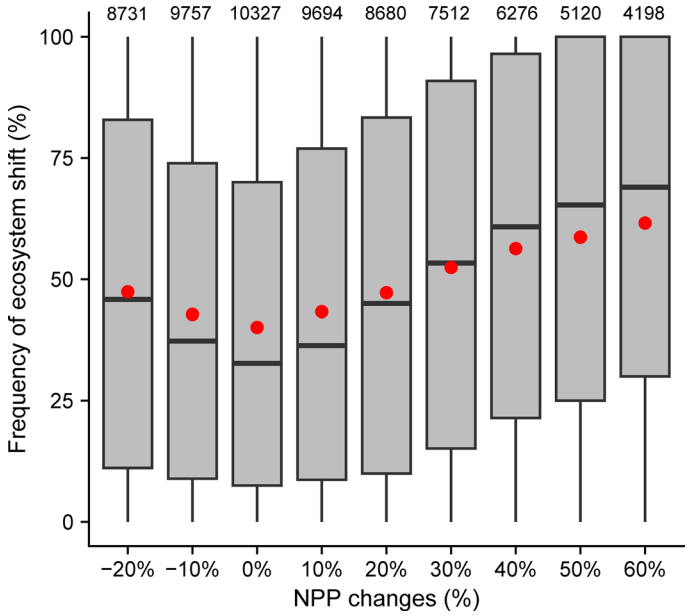

Extended Data Fig. 7 | Percentage shift of ecosystem types induced by plant productivity changes under warming. The percentage shift is calculated as the fraction of ecosystem types at each profile location in the W+NPP group that are different from the ecosystem type in the A group. Boxplots show the median and interquartile range (IQR), with whiskers extending to the most extreme values within the 1.5 times of IQR. The red point represents the average. The numbers at the top of the box are the sample size.